Inorganic Chemistry
Cite This: Inorg. Chem. 2019, 58, 8910−8914
Communication
pubs.acs.org/IC

Efficient Electroreduction CO_2 to CO over MnO_2 Nanosheets

Xianyun Peng,[†,#] Ying Chen,[†,#] Yuying Mi,[†] Longchao Zhuo,[‡] Gaocan Qi,[*,§] Junqiang Ren,[∥] Yuan Qiu,[†] Xijun Liu,[*,†] and Jun Luo[†]

[†]Center for Electron Microscopy and Tianjin Key Lab of Advanced Functional Porous Materials, Institute for New Energy Materials and Low-Carbon Technologies, School of Materials Science and Engineering, Tianjin University of Technology, Tianjin 300384, China

[‡]School of Materials Science and Engineering, Xi'an University of Technology, Xi'an 710048, China

[§]School of Materials Science and Engineering, Tianjin University of Technology, Tianjin 300384, China

[∥]State Key Laboratory of Advanced Processing and Recycling of Nonferrous Metals, Lanzhou University of Technology, Lanzhou 730050, China

Supporting Information

ABSTRACT: As a critical alternative step for the synthesis of important chemical feedstocks and complex carbon-based fuels, the electrochemical transformation of CO_2 into CO holds great significance for the chemical industry. Here, MnO_2 nanosheets array supported nickel foam has been synthesized and adopted as a binder-free catalyst for electrochemical CO_2 reduction reaction (CO_2RR). The well-distributed nanosheets of MnO_2 impart a much higher density of accessible active sites for CO_2RR, enabling the selective CO_2 reduction to CO with a large current density (14.1 mA cm^{-2}), excellent Faradaic efficiency (71%) and high electrochemical stability (10 h). This work first demonstrates the great potential of Mn-based oxides for electrocatalytic transformation of CO_2 to valuable products.

Atmosphere emission of carbon dioxide (CO_2) is becoming a serious threat to the environment with the ever-growing worldwide consumption of fossil fuels. The conversion of excess CO_2 into valuable chemicals has attracted extensive research for meeting the demands of sustainable utilization of the scarce fuels and chemicals.[1−9] Currently, the electrochemical CO_2 reduction reaction (CO_2RR) into carbon-based feedstocks and fuels under ambient conditions using the renewable electricity sources is considered as a promising method for curbing CO_2 emissions while generating valuable fuels and chemicals.[10−15] Among the electroreduction products, CO is a promising one, as CO is a gas under ambient conditions and can be easily separated from the electrolytes for further utilization.[16−18] More importantly, CO is an important chemical that can be applied in a wide range application. Especially, as a key component of syngas, CO can be used to prepare a mass of basic chemical products and intermediates by using Fischer−Tropsch chemistry.[19] It is worth noting that traditional CO_2 hydrogenation to produce CO is an equilibrium-limited endothermic reaction, which requires a high temperature of more than 400 °C.[20] By contrast, selective electrochemical CO_2RR can be performed under ambient conditions and obtain high activity and selectivity for CO production.

On the way to scaling up CO_2RR for practical CO_2 electrolysis, although noble metals (e.g., Au, Ag, Pd) have been developed to deliver a high activity and selectivity for CO production in aqueous solution (Table S1), the rarity and high cost of precious metal-based electrocatalysts limit their large-scale applications. It is urgent to develop cost-effective and high-performance electrocatalysts. As a cost-effective alternative, an earth-rich transition metal oxide provides an interesting paradigm for CO_2-to-CO conversion. However, to date, only two metal oxides (ZnO and $ZnGa_2O_4$) have been designed as efficient electrocatalysts for the conversion of CO_2 to CO.[21,22] Despite these breakthroughs, high Faradaic efficiency (FE) is typically achieved at the expense of low CO reduction current. Hence, the design of highly selective and energy-efficient catalysts is highly desirable to enable both high FE and reduction current for CO production at a low overpotential.

Manganese oxide, one important transition metal oxide with merits of high redox potential, environmentally friendliness, and rich reserves,[23−26] holds great promise for widespread application as electrode materials,[27,28] sorbents,[29−31] and catalysts.[32−34] In this communication, for the first time, we demonstrate our recent finding that MnO_2 nanosheets supported on nickel foam (MnO_2−NS/NF) behave as a catalyst toward efficient electrochemical CO_2 reduction with excellent activity, selectivity, and stability for CO production under ambient conditions. In 0.1 M $KHCO_3$ aqueous solution, the MnO_2−NS/NF catalyst achieved a high FE of 71% at −0.95 V versus the reversible hydrogen electrode (vs RHE). Additionally, this electrochemical system also offers long-term stability for the transformation of CO_2 to CO over the MnO_2−NS/NF catalyst.

MnO_2−NS/NF was prepared by the one-step hydrothermal method shown in Figure 1a. Typically, a piece of cleaned nickel foam was put into a Teflon-lined stainless steel autoclave and then 30 mL homogeneous $KMnO_4$ aqueous solution was added. Afterward, the autoclave was sealed and maintained at 160 °C for 24 h to obtain MnO_2−NS/NF. In this synthesis process, MnO_2−NS/NF was produced via self-decomposition of

Received: April 10, 2019
Published: May 15, 2019

DOI: 10.1021/acs.inorgchem.9b01018
Inorg. Chem. 2019, 58, 8910−8914

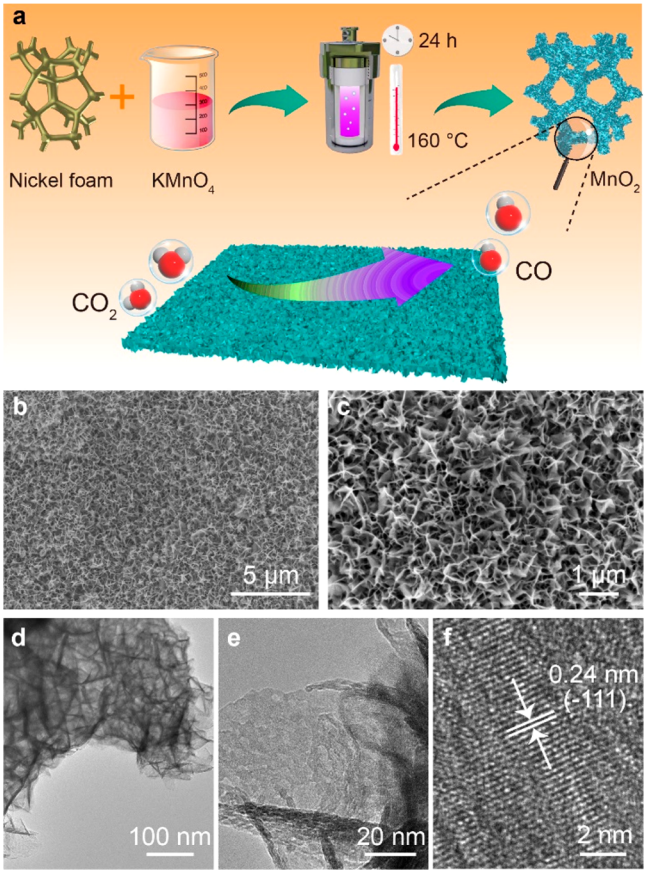

Figure 1. (a) Schematic of the synthetic procedure of MnO_2−NS/NF; (b, c) SEM images; (d, e) TEM images; (f) HR-TEM image.

$KMnO_4$ in the progress of hydrothermal reaction without any surfactant.

Scanning electron microscopy (SEM) images in Figures 1b,c and S1 show the representative MnO_2 nanosheet directly grown on the Ni foam on a large scale. The anisotropic growth enabled MnO_2−NS/NF to be well interconnected with each other, forming the uniform arrays with a three-dimensional (3D) hierarchical structure. This 3D structure can significantly ensure high accessibility to the electrolyte and allow fast ion diffusion by shortening the diffusion paths, resulting in significant improvement of the electrochemical CO_2RR properties.[15,35,36] The detailed microstructures of the MnO_2 nanosheets were further characterized by transmission electron microscopy (TEM). As shown in Figures 1d,e and S2, the MnO_2 nanosheets are connected to each other to form a 3D structure. AFM images and the corresponding height profiles in Figure S3 demonstrate that the MnO_2 nanosheets have an approximate average thickness of 4 nm. Besides, the N_2 adsorption−desorption test indicated that the as-synthesized MnO_2 nanosheets possess a surface area as high as 387.4 m^2 g^{-1} and a pore size of 1.1 nm (Figure S4). The large surface area and the porous structure would be beneficial to the exposure of more active sites and rapid transportation of CO_2RR relevant species. Moreover, the high-resolution TEM (HR-TEM) showed clear lattice fringes with an interplanar spacing of 0.24 nm, which can be assigned to the typical (−111) plane of birnessite-type MnO_2 (Figure 1f).

The crystalline structure of MnO_2−NS/NF was characterized by XRD analysis. As shown in Figure 2a, four diffraction peaks located at 12.5°, 25.3°, 36.2°, and 65.6° agreed well with the (001), (002), ($\bar{1}$11), and (020) planes of the monoclinic

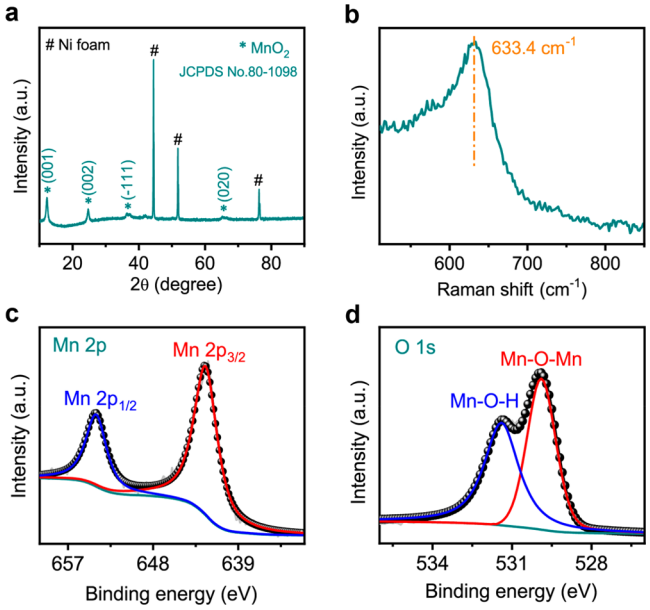

Figure 2. Structural characterization of the as-prepared MnO_2−NS/NF. (a) XRD pattern. (b) Raman spectrum. High-resolution XPS spectra of (d) Mn 2p and (d) O 1s.

structure of MnO_2 phase (JCPDS No. 80-1098) with lattice constants of a = 0.5149 nm, b = 0.2842 nm, and c = 0.7047 nm.[37] The strong peaks marked with "#" are ascribed to the Ni foam. Furthermore, the Raman spectrum of MnO_2−NS/NF (Figure 2b) shows one distinct peak located at 633.4 cm^{-2} can be assigned to the symmetric stretching vibration of the Mn−O bond parallel to the basal (001) plane.[38,39] Furthermore, the composition information on MnO_2−NS/NF was investigated by X-ray photoelectron spectroscopy (XPS). As results, the high-resolution Mn 2p XPS spectrum (Figure 2c) displays two representative characteristic peaks at 642.4 and 653.9 eV corresponding to the Mn $2p_{3/2}$ and Mn $2p_{1/2}$, respectively, which indicate a +4 oxidation state for Mn in MnO_2−NS/NF.[40,41] For the O 1s spectrum (Figure 2d), it can be deconvoluted into two components assigning to two different types of oxygen bonds: Mn−O−Mn and Mn−O−H at 529.9 and 531.4 eV, respectively.[40,42] XPS quantitative analysis indicated that the atomic ratio of Mn to O was approximately 0.5. These gave strong evidenced of the successful growth of MnO_2 nanosheets on nickel foam.

The electrochemical CO_2RR performances of the MnO_2−NS/NF catalysts were evaluated in high-purity CO_2-saturated 0.1 M $KHCO_3$ aqueous solution by using a typical three-electrode system, where the counter electrode, reference electrode, and separator were Pt foil, the saturated calomel electrode (SCE), and a Nafion-115 proton exchange membrane, respectively. For comparison, commercial MnO_2 was also tested under the same conditions (Figures S5 and S6). First, linear sweep voltammetry (LSV) was performed to examine the CO_2RR catalytic activity of the catalysts. As revealed in Figure 3a, the MnO_2−NS/NF catalyst shows a much higher current density (32.6 mA cm^{-2} at −1.1 V) in CO_2-saturated aqueous solution than that of N_2 and Ar (Figure S7), demonstrating that the high activity of MnO_2−NS/NF catalyst toward the electrochemical CO_2 reduction.[43]

To further investigate the electroreduction CO_2 performance of MnO_2−NS/NF, the reduction products were identified with a chrono-amperometry method after 2 h of electrolysis for each

DOI: 10.1021/acs.inorgchem.9b01018
Inorg. Chem. 2019, 58, 8910−8914

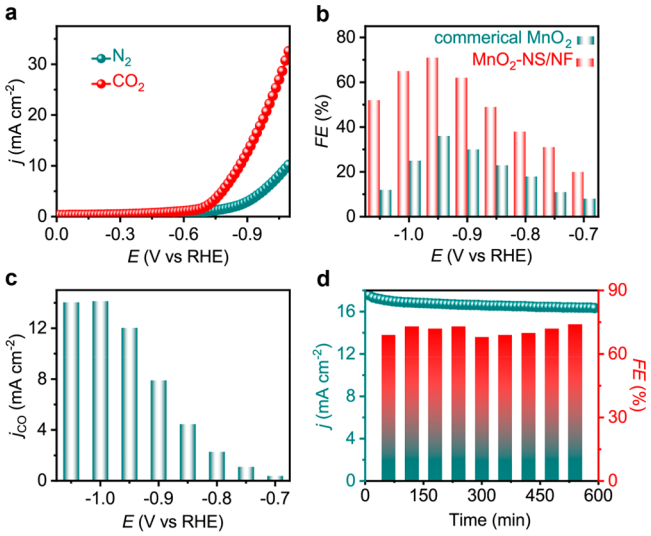

Figure 3. Electrochemical CO_2RR performance characterization. (a) LSV of the MnO_2−NS/NF catalyst performed in CO_2-saturated and N_2-saturated 0.1 M $KHCO_3$ electrolyte at a scan rate of 10 mV s^{-1}. (b) FE for the production of CO at different applied potentials. (c) Current density for CO production at the set potentials. (d) Long-term stability of MnO_2−NS/NF operated at the applied potential of −0.95 V for more than 600 min continuous electrolysis.

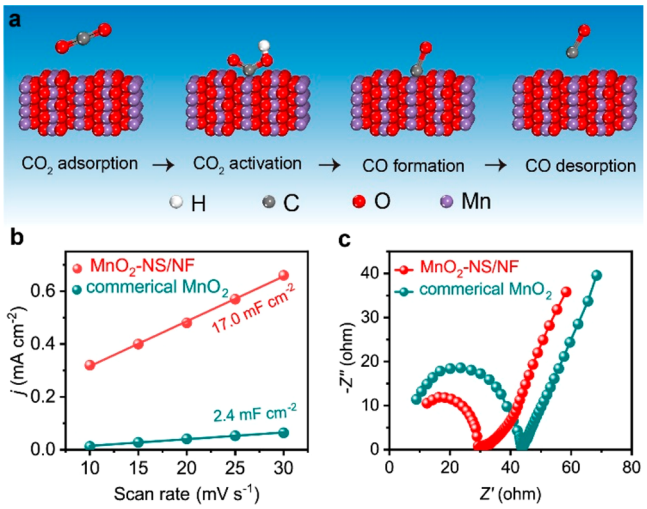

Figure 4. (a) Scheme of the CO_2 reduction into CO over MnO_2−NS/NF. (b) Plots of the current density versus the scan rate for MnO_2−NS/NF and commercial MnO_2. (c) Nyquist plots of MnO_2−NS/NF and commercial MnO_2.

applied potential. The products were quantified by an ^1H nuclear magnetic resonance (NMR) spectrometer and an online gas chromatography (GC). As observed, the MnO_2−NS/NF catalyst exhibited a higher FE for CO production with respect to the commercial MnO_2 at each applied potential (Figure 3b). No liquid products were detected by ^1H NMR. Specifically, with the potential increases from −0.7 to −0.95 V, the FE of CO increases gradually. At −0.95 V, the maximum FE of the MnO_2−NS/NF catalyst for CO production can reach up to 71%, whereas the FE of the commercial MnO_2 was 36%. At each applied potential, the MnO_2−NS/NF catalyst exhibited a higher current density toward electrochemical CO_2 reduction to CO production (Figure 3c). Typically, at −1.05 V, the current density of the MnO_2−NS/NF catalyst for CO production was up to 14.1 mA cm^{-2}. In addition, stability was another crucial factor in evaluating CO_2RR performance. To test the operational stability of the MnO_2−NS/NF catalysts, CO_2RR was carried out over an extended period of time (600 min). As shown in Figure 3d, the MnO_2−NS/NF catalyst displayed a stable current density and FE during the long-term continuous stability test, indicating the preferable durability of the catalyst. Moreover, MnO_2−NS/NF also kept its original morphology (Figure S8) and crystalline structure (Figure S9) after 10 h of electrolysis.

The electrochemical CO_2RR mechanism for CO production over the MnO_2−NS/NF catalyst can be interpreted by two coupled electron−proton transfer reactions. As shown in Figure 4a, the CO_2 molecule is first adsorbed and protonated on MnO_2−NS/NF by combining with one proton (H^+) and one electron (e^-) to form the important intermediate (COOH*). Subsequently, the second electron−proton pair is transferred to achieve adsorbed CO*. Finally, the CO* desorbed from the surface of the catalyst and thus produced CO gas. According to previous reports, the second reaction can occur naturally with thermal access, while the reaction rate of electrochemical CO_2RR is determined by the first step of CO_2 adsorption or the last step of CO desorption.

To gain insight into the origin of catalytic activity of the MnO_2−NS/NF catalyst for the production of CO production, the electrochemically active surface area (ECSA) was analyzed. In general, the ECSA was evaluated by the electrochemical double layer capacitance (C_{dl}) using typical cyclic voltammetry (CV),[44,45] which was measured under a CO_2-saturated 0.1 M $KHCO_3$ electrolyte at scan rates of 10, 15, 20, 25, and 30 mV s^{-1}, respectively (Figure S10). As shown in Figure 4b, the C_{dl} of MnO_2−NS/NF (17.0 mF cm^{-2}) is significantly higher than that of commercial MnO_2 (2.4 mF cm^{-2}). This is mainly due to the direct growth of MnO_2−NS/NF from the underlying conductive substrate, which eliminates the use of any binders. Besides, the large C_{dl} of MnO_2−NS/NF implied a higher surface area and more exposed active sites, which is beneficial to enhance the electrochemical CO_2 reduction activity. Additionally, the electrochemical impedance spectroscopy (EIS) is a powerful tool for studying reaction kinetics in the catalytic process. Typically, the Nyquist plots (Figure 4c) were composed of one semicircle and a straight line at high-frequency and low-frequency regions, respectively. Specifically, MnO_2−NS/NF has a smaller radius of the semicircle than that of commercial MnO_2, manifesting the fast electron transfer rate across the electrode−electrolyte interface and faster CO_2 catalytic kinetics of MnO_2−NS/NF.[36,46] Meantime, the Nyquist plots for the MnO_2−NS/NF electrode before (Figure 4c) and after (Figure S11) stability test are similar. This also demonstrated that the MnO_2−NS/NF catalyst had excellent stability, which agreed well with the characterization results of the morphology and crystalline structure of MnO_2−NS/NF.

In summary, nickel foam-supported MnO_2 nanosheets were prepared and applied to the electrochemical CO_2 reduction reaction. Benefiting from the abundant exposed active sites, the MnO_2 nanosheets enabled the efficient and robust CO_2 reduction to CO with the combination of large reduction current density (14.1 mA cm^{-2} at −1.0 V), high selectivity (FE of 71%), and great durability (no activity or selectivity loss for 10 h). The high performance was among the best results reported for aqueous CO_2RR on metal oxide-based electrocatalysts and was comparable to the previously studied noble metal catalysts

DOI: 10.1021/acs.inorgchem.9b01018
Inorg. Chem. 2019, 58, 8910−8914

(such as Au, Ag, and Pd). Our work offers a new opportunity for the application of abundant manganese for CO_2 conversion.

■ ASSOCIATED CONTENT

Supporting Information

The Supporting Information is available free of charge on the ACS Publications website at DOI: 10.1021/acs.inorgchem.9b01018.

Synthesis of MnO_2 nanosheets supported on nickel foam, material characterization, electrochemical CO_2 reduction measurements, products analysis, SEM, TEM, and AFM images, BET characterizations, XRD patterns, LSV of the MnO_2-NS/NF catalyst, CV curves, Nyquist plots, table of CO eveolution data (PDF)

■ AUTHOR INFORMATION

Corresponding Authors

*E-mail: gaocanqi@tjut.edu.cn.
*E-mail: xjliu@tjut.edu.cn.

ORCID

Longchao Zhuo: 0000-0003-3396-3893
Xijun Liu: 0000-0002-2624-6901
Jun Luo: 0000-0001-5084-2087

Author Contributions

#These authors contributed equally to this work.

Notes

The authors declare no competing financial interest.

■ ACKNOWLEDGMENTS

This work was financially supported by National Key R&D Program of China (2017YFA0700104), National Science Fund for Distinguished Young Scholars (51825102), National Natural Science Foundation of China (51761165012, 51671145, 21601136, 21677010, 21603161, and 21501132), National Program for Thousand Young Talents of China, and Tianjin Municipal Science and Technology Commission (15JCYBJC52600).

■ REFERENCES

(1) Zheng, Y.; Vasileff, A.; Zhou, X.; Jiao, Y.; Jaroniec, M.; Qiao, S. Z. Understanding the roadmap for electrochemical reduction of CO_2 to multi-carbon oxygenates and hydrocarbons on copper-based catalysts. *J. Am. Chem. Soc.* **2019**, DOI: 10.1021/jacs.9b02124.

(2) Vasileff, A.; Xu, C.; Jiao, Y.; Zheng, Y.; Qiao, S.-Z. Surface and interface engineering in copper-based bimetallic materials for selective CO_2 electroreduction. *Chem.* **2018**, *4*, 1809−1831.

(3) Jiao, Y.; Zheng, Y.; Chen, P.; Jaroniec, M.; Qiao, S. Z. Molecular scaffolding strategy with synergistic active centers to facilitate electrocatalytic CO_2 reduction to hydrocarbon/alcohol. *J. Am. Chem. Soc.* **2017**, *139*, 18093−18100.

(4) Chen, P.; Jiao, Y.; Zhu, Y.-H.; Chen, S.-M.; Song, L.; Jaroniec, M.; Zheng, Y.; Qiao, S.-Z. Syngas production from electrocatalytic CO_2 reduction with high energetic efficiency and current density. *J. Mater. Chem. A* **2019**, *7*, 7675−7682.

(5) Wang, W.; Shang, L.; Chang, G.; Yan, C.; Shi, R.; Zhao, Y.; Waterhouse, G. I. N.; Yang, D.; Zhang, T. Intrinsic carbon-defect-driven electrocatalytic reduction of carbon dioxide. *Adv. Mater.* **2019**, *31*, 1808276.

(6) Zhao, Y.; Chang, C.; Teng, F.; Zhao, Y.; Chen, G.; Shi, R.; Waterhouse, G. I. N.; Huang, W.; Zhang, T. Defect-engineered ultrathin δ-MnO_2 nanosheet arrays as bifunctional electrodes for efficient overall water splitting. *Adv. Energy. Mater.* **2017**, *7*, 1700005.

(7) Zhao, Y.; Waterhouse, G. I. N.; Chen, G.; Xiong, X.; Wu, L. Z.; Tung, C. H.; Zhang, T. Two-dimensional-related catalytic materials for solar-driven conversion of CO_x into valuable chemical feedstocks. *Chem. Soc. Rev.* **2019**, *48*, 1972−2010.

(8) Shang, X.; Dong, B.; Chai, Y.-M.; Liu, C.-G. In-situ electrochemical activation designed hybrid electrocatalysts for water electrolysis. *Sci. Bull.* **2018**, *63*, 853−876.

(9) Zhu, D. D.; Liu, J. L.; Qiao, S. Z. Recent advances in inorganic heterogeneous electrocatalysts for reduction of carbon dioxide. *Adv. Mater.* **2016**, *28*, 3423−3452.

(10) Huo, Y.; Peng, X.; Liu, X.; Li, H.; Luo, J. High selectivity toward C_2H_4 production over Cu particles supported by butterfly-wing-derived carbon frameworks. *ACS Appl. Mater. Interfaces* **2018**, *10*, 12618−12625.

(11) Liu, X.; Yang, H.; He, J.; Liu, H.; Song, L.; Li, L.; Luo, J. Highly active, durable ultrathin $MoTe_2$ layers for the electroreduction of CO_2 to CH_4. *Small* **2018**, *14*, 1704049.

(12) Mi, Y.; Peng, X.; Liu, X.; Luo, J. Selective formation of C2 products from electrochemical CO_2 reduction over $Cu_{1.8}Se$ nanowires. *ACS Appl. Energy Mater.* **2018**, *1*, 5119−5123.

(13) Mi, Y.; Shen, S.; Peng, X.; Bao, H.; Liu, X.; Luo, J. Selective electroreduction of CO_2 to C2 products over Cu_3N-derived Cu nanowires. *ChemElectroChem* **2019**, *6*, 2393−2397.

(14) Shen, S.; He, J.; Peng, X.; Xi, W.; Zhang, L.; Xi, D.; Wang, L.; Liu, X.; Luo, J. Stepped surface-rich copper fiber felt as an efficient electrocatalyst for the CO_2RR to formate. *J. Mater. Chem. A* **2018**, *6*, 18960−18966.

(15) Zhao, Z.; Peng, X.; Liu, X.; Sun, X.; Shi, J.; Han, L.; Li, G.; Luo, J. Efficient and stable electroreduction of CO_2 to CH_4 on CuS nanosheet arrays. *J. Mater. Chem. A* **2017**, *5*, 20239−20243.

(16) Ma, M.; Trzesniewski, B. J.; Xie, J.; Smith, W. A. Selective and efficient reduction of carbon dioxide to carbon monoxide on oxide-derived nanostructured silver electrocatalysts. *Angew. Chem., Int. Ed.* **2016**, *55*, 9748−9752.

(17) Verma, S.; Hamasaki, Y.; Kim, C.; Huang, W.; Lu, S.; Jhong, H.-R. M.; Gewirth, A. A.; Fujigaya, T.; Nakashima, N.; Kenis, P. J. A. Insights into the low overpotential electroreduction of CO_2 to CO on a supported gold catalyst in an alkaline flow electrolyzer. *ACS Energy Lett.* **2018**, *3*, 193−198.

(18) Won, D. H.; Shin, H.; Koh, J.; Chung, J.; Lee, H. S.; Kim, H.; Woo, S. I. Highly efficient, selective, and stable CO_2 electroreduction on a hexagonal Zn catalyst. *Angew. Chem., Int. Ed.* **2016**, *55*, 9297−9300.

(19) Khodakov, A. Y.; Chu, W.; Fongarland, P. Advances in the development of novel cobalt Fischer−Tropsch catalysts for synthesis of long-chain hydrocarbons and clean fuels. *Chem. Rev.* **2007**, *107*, 1692−1744.

(20) Centi, G.; Perathoner, S. Opportunities and prospects in the chemical recycling of carbon dioxide to fuels. *Catal. Today* **2009**, *148*, 191−205.

(21) Geng, Z.; Kong, X.; Chen, W.; Su, H.; Liu, Y.; Cai, F.; Wang, G.; Zeng, J. Oxygen vacancies in ZnO nanosheets enhance CO_2 electrochemical reduction to CO. *Angew. Chem., Int. Ed.* **2018**, *57*, 6054−6059.

(22) Zhao, M.; Gu, Y.; Chen, P.; Xin, Z.; Zhu, H.; Wang, B.; Zhu, K.; Yan, S.; Zou, Z. Highly selective electrochemical CO_2 reduction to CO using a redox-active couple on low-crystallinity mesoporous $ZnGa_2O_4$ catalyst. *J. Mater. Chem. A* **2019**, *7*, 9316−9323.

(23) Sun, W.; Wang, F.; Hou, S.; Yang, C.; Fan, X.; Ma, Z.; Gao, T.; Han, F.; Hu, R.; Zhu, M.; Wang, C. Zn/MnO_2 battery chemistry with H^+ and Zn^{2+} coinsertion. *J. Am. Chem. Soc.* **2017**, *139*, 9775−9778.

(24) Wei, W.; Cui, X.; Chen, W.; Ivey, D. G. Manganese oxide-based materials as electrochemical supercapacitor electrodes. *Chem. Soc. Rev.* **2011**, *40*, 1697−1721.

(25) Ren, Y.; Yan, N.; Wen, Q.; Fan, Z.; Wei, T.; Zhang, M.; Ma, J. Graphene/δ-MnO_2 composite as adsorbent for the removal of nickel ions from wastewater. *Chem. Eng. J.* **2011**, *175*, 1−7.

(26) Sun, W.; Zhou, Z.; Zaman, W. Q.; Cao, L. M.; Yang, J. Rational manipulation of IrO_2 lattice strain on alpha-MnO_2 nanorods as a highly

DOI: 10.1021/acs.inorgchem.9b01018
Inorg. Chem. 2019, 58, 8910−8914

efficient water-splitting catalyst. *ACS Appl. Mater. Interfaces* **2017**, *9*, 41855−41862.
(27) Zhao, T.; Yao, Y.; Wang, M.; Chen, R.; Yu, Y.; Wu, F.; Zhang, C. Preparation of MnO_2-modified graphite sorbents from spent Li-Ion batteries for the treatment of water contaminated by lead, cadmium, and silver. *ACS Appl. Mater. Interfaces* **2017**, *9*, 25369−25376.
(28) Liu, S.; Wang, G.; Tu, F.; Xie, J.; Yang, H. Y.; Zhang, S.; Zhu, T.; Cao, G.; Zhao, X. Au-nanocrystals-decorated delta-MnO_2 as an efficient catalytic cathode for high-performance Li-O_2 batteries. *Nanoscale* **2015**, *7*, 9589−9596.
(29) Tan, Y.; Xu, C.; Chen, G.; Fang, X.; Zheng, N.; Xie, Q. Facile synthesis of manganese-oxide-containing mesoporous nitrogen-doped carbon for efficient oxygen reduction. *Adv. Funct. Mater.* **2012**, *22*, 4584−4591.
(30) Zhao, Y.; Chang, C.; Teng, F.; Zhao, Y.; Chen, G.; Shi, R.; Waterhouse, G. I. N.; Huang, W.; Zhang, T. Defect-engineered ultrathin δ-MnO_2 nanosheet arrays as bifunctional electrodes for efficient overall water splitting. *Adv. Energy Mater.* **2017**, *7*, 1700005.
(31) Walanda, D. K.; Lawrance, G. A.; Donne, S. W. Hydrothermal MnO_2: synthesis, structure, morphology and discharge performance. *J. Power Sources* **2005**, *139*, 325−341.
(32) Liu, B.; Sun, Y.; Liu, L.; Xu, S.; Yan, X. Advances in manganese-based oxides cathodic electrocatalysts for Li-air batteries. *Adv. Funct. Mater.* **2018**, *28*, 1704973.
(33) Rice, D. B.; Massie, A. A.; Jackson, T. A. Manganese-oxygen intermediates in O-O bond activation and hydrogen-atom transfer reactions. *Acc. Chem. Res.* **2017**, *50*, 2706−2717.
(34) Tang, Y.; Zheng, S.; Xu, Y.; Xiao, X.; Xue, H.; Pang, H. Defect-engineered ultrathin δ-MnO_2 nanosheet arrays as bifunctional electrodes for efficient overall water splitting. *Energy Storage Mater.* **2018**, *12*, 284−309.
(35) Deng, S.; Zhong, Y.; Zeng, Y.; Wang, Y.; Yao, Z.; Yang, F.; Lin, S.; Wang, X.; Lu, X.; Xia, X.; Tu, J. Directional construction of vertical nitrogen-doped 1T-2H $MoSe_2$/graphene shell/core nanoflake arrays for efficient hydrogen evolution reaction. *Adv. Mater.* **2017**, *29*, 1700748.
(36) Xie, D.; Xia, X.; Zhong, Y.; Wang, Y.; Wang, D.; Wang, X.; Tu, J. Exploring advanced sandwiched arrays by vertical graphene and N-doped carbon for enhanced sodium storage. *Adv. Energy Mater.* **2017**, *7*, 1601804.
(37) Huang, M.; Zhao, X. L.; Li, F.; Zhang, L. L.; Zhang, Y. X. Facile synthesis of ultrathin manganese dioxide nanosheets arrays on nickel foam as advanced binder-free supercapacitor electrodes. *J. Power Sources* **2015**, *277*, 36−43.
(38) Julien, C. Raman spectra of birnessite manganese dioxides. *Solid State Ionics* **2003**, *159*, 345−356.
(39) Miao, L.; Nie, Q.; Wang, J.; Zhang, G.; Zhang, P. Ultrathin MnO_2 nanosheets for optimized hydrogen evolution via formaldehyde reforming in water at room temperature. *Appl. Catal., B* **2019**, *248*, 466−476.
(40) Xia, H.; Feng, J.; Wang, H.; Lai, M. O.; Lu, L. MnO_2 nanotube and nanowire arrays by electrochemical deposition for supercapacitors. *J. Power Sources* **2010**, *195*, 4410−4413.
(41) Wu, Z.-S.; Ren, W.; Wang, D.-W.; Li, F.; Liu, B.; Cheng, H.-M. High-energy MnO_2 nanowire/graphene and graphene asymmetric electrochemical capacitors. *ACS Nano* **2010**, *4*, 5835−5842.
(42) Wei, W.; Cui, X.; Chen, W.; Ivey, D. G. Phase-controlled synthesis of MnO_2 nanocrystals by anodic electrodeposition: implications for high-rate capability electrochemical supercapacitors. *J. Phys. Chem. C* **2008**, *112*, 15075−15083.
(43) Wang, H.; Jia, J.; Song, P.; Wang, Q.; Li, D.; Min, S.; Qian, C.; Wang, L.; Li, Y. F.; Ma, C.; Wu, T.; Yuan, J.; Antonietti, M.; Ozin, G. A. Efficient electrocatalytic reduction of CO_2 by nitrogen-doped nanoporous carbon/carbon nanotube membranes: A step towards the electrochemical CO_2 refinery. *Angew. Chem., Int. Ed.* **2017**, *56*, 7847−7852.
(44) Qiao, J.; Liu, Y.; Hong, F.; Zhang, J. A review of catalysts for the electroreduction of carbon dioxide to produce low-carbon fuels. *Chem. Soc. Rev.* **2014**, *43*, 631−675.
(45) An, T.; Wang, Y.; Tang, J.; Wei, W.; Cui, X.; Alenizi, A. M.; Zhang, L.; Zheng, G. Interlaced NiS_2-MoS_2 nanoflake-nanowires as efficient hydrogen evolution electrocatalysts in basic solutions. *J. Mater. Chem. A* **2016**, *4*, 13439−13443.
(46) Shen, S.; Xia, X.; Zhong, Y.; Deng, S.; Xie, D.; Liu, B.; Zhang, Y.; Pan, G.; Wang, X.; Tu, J. Implanting niobium carbide into trichoderma spore carbon: a new advanced host for sulfur cathodes. *Adv. Mater.* **2019**, *31*, 1900009.

DOI: 10.1021/acs.inorgchem.9b01018
Inorg. Chem. 2019, 58, 8910−8914